Pergamon

0301-9322(95)00017-8

*Int. J. Multiphase Flow* Vol. 21, No. 5, pp. 919–927, 1995

0301-9322/95 $9.50 + 0.00

# BRIEF COMMUNICATION

# MODULATION OF SHEAR LAYER THICKNESS DUE TO LARGE BUBBLES

E. LOTH and M. S. CEBRZYNSKI

Department of Aeronautical and Astronautical Engineering, University of Illinois at Urbana-Champaign, Urbana, IL 61801, U.S.A.

*(Received 20 January 1994; in revised form 16 February 1995)*

## 1. INTRODUCTION

Turbulent two-phase flow is not fully understood in part due to the flowfield's extreme complexity, and the interactions between the turbulent continuous phase (gas, liquid, etc.) and the dispersed phase (bubbles, particles or droplets). There are two general classifications of turbulent interactions studied in multiphase flow: turbulence modulation—the effect of the dispersed phase on the continuous phase turbulence, and turbulent dispersion—the effect of the continuous phase motion on the dispersed phase's behavior (trajectory, distribution). This study focused on the effects of turbulence modulation in modifying the passive scalar thickness of a free shear layer of tap water when subjected to large air bubbles (diameters $>1$ mm). Such large bubbles may be distinct in two regards: they are typified by shape deformation (ellipsoidal for the present study) which results in both modified drag relations and a non-rectilinear trajectory, and their size may also approach the integral scale of the surrounding fluid turbulence potentially which may result in strong interactions between the bubble wakes and the shear layer coherent structures.

To understand turbulence modulation, we may attempt to separate the overall effect into two categories as per Lopez de Bertodano *et al.* (1994): shear induced turbulence modulation (SITM) and pseudo-turbulence modulation (PTM). SITM is related to the modification of the shear generated bulk transport of mass and momentum of the continuous fluid. Whereas, PTM is related solely to the dispersed phase perturbations in the flowfield which include the motion, the wakes and the surrounding potential flow disturbance of the dispersed phase. For example, PTM for large bubbles can dramatically increase velocity fluctuation levels even at moderate void fractions, e.g. 2% (Theofanous & Sullivan 1982), but such random arrival perturbations do not necessarily constitute a turbulent flow in and of themselves, and therefore should not be considered a modification of the underlying shear driven turbulence. However, PTM may be difficult to discriminate experimentally from SITM for Stokes numbers near unity due to the proximity of the wake and eddy frequencies. In addition, for large test sections and moderate void fractions as used herein, LDA or PIV access is difficult (Roig *et al.* 1993).

The large scale coherent structures arising from Kelvin–Helmholtz shear instabilities in a fully developed single-phase free shear layer have been shown to govern the bulk entrainment of non-turbulent fluid into the shear layer, referred to as induction (Dimotakis 1991), and dominate the turbulent energy spectra (which is plainly shear induced). For bubbly shear layers, the large scale structures (as opposed to the random bubble fluctuations associated with PTM) similarly control the entrainment and shear induced turbulence. The net turbulent energy of the large scale structures is related to the eddy strength (governed by the velocity difference across the shear layer, $\Delta V = V_1 - V_2$), coherency, and size. Thus, changes in the shear layer thickness ($\delta$) for a bubbly flow, which result from changes in the eddy sizes, indicate modifications of entrainment and a macroscopic result of shear induced turbulent transport modulation. While changes in coherent structures have been measured for other turbulent two-phase flows, e.g. particle induced

modifications of momentum transport due to changes in boundary layer ejection frequencies (Hetsroni 1993), there have been no previous detailed measurements of $\delta$ modifications for bubbly shear layers other than a study by Roig *et al.* (1993), which documented an increase in thickness for one flow condition.

Two non-dimensional parameters, which may reflect important regimes of two-phase interactions, are the dispersed phase time and length scale ratios. The time scale ratio is often referred to as the Stokes number (St), which is defined as the ratio of the aerodynamic response time of a bubble ($\tau_b$) to the characteristic time scale of the convecting fluid ($\tau_f$). A $St \ll 1$ indicates bubbles for which drag dominates and which tend to behave as passive tracers, while increasing Stokes numbers represent bubbles which show less tendency to follow the turbulent eddies and more tendency to be driven by pressure gradient forces. The pressure gradients may be both centripetal and hydrostatic, the ratio of which for an irrotational vortex can be described with the eddy Froude number ($Fr_\delta = \Delta V^2/g\delta$), where $g$ is gravity. This parameter was previously identified by non-dimensionalizing the bubble momentum equation for a Stuart vortex (Tio *et al.* 1993). The bubble time scale is defined as the mean relative velocity ($V_{rel}$) and apparent mass divided by bubble drag, and is given by [8] of Stewart & Crowe (1993) as $4C_v d_b/(3V_{rel}C_d)$, where $C_v$ is the coefficient of virtual mass, $d_b$ is the bubble diameter, and $C_d$ is the drag coefficient. If $C_d$ is not based on the Stokesian drag law, as is the case herein, a "modified" Stokes number ($St_m$) is more appropriate. Based on direct measurements of relative velocity (in both still and turbulent flow) for the present 2 and 4 mm bubbles, we find $V_{rel}$ is approximately equal to the terminal velocity of 34.8 and 30.3 cm/s respectively. This resulted in a $C_d$ which increases with bubble Reynolds number ($Re_b$), due to the large bubble diameters. Based on results from Jiang *et al.* (1993) and Lopez de Bertodano *et al.* (1994), the $C_v$ was linearly interpolated as 1.4 and 2.0, respectively. Rewriting the bubble time scale as $C_v V_{rel}/g$, yields 0.050 and 0.062 s, respectively. The fluid time scale is typically given as $\delta/\Delta V$. However, for high bubble velocities it may be more appropriate to write $\tau_f$ as the timescale for bubble–eddy interaction, i.e. the minimum of $\delta/\Delta V$ and $\delta/V_{rel}$.

The dispersion length scale ratio ($\beta$) is defined as the ratio of the dispersed phase diameter ($d_b$) to the length scale associated with the integral scale of a mixing layer ($\Lambda$). This ratio may be important, since a survey by Gore & Crowe (1989) noted that smaller particles, bubbles or drops ($\beta < 0.07$) in a turbulent flow can reduce the turbulence intensity, whereas larger ones ($\beta > 0.07$) tend to enhance the intensity. It was proposed that a small dispersed phase will tend to follow the eddy and absorb, through drag, some of the turbulent energy of the eddy and the overall turbulence will be reduced, whereas a large dispersed phase will tend to create wakes, which may increase the overall turbulent intensity of continuous fluid. However, other data sets were found to conflict with the above trend (Davis 1993). Several models to quantify the resulting pointwise turbulent energy modification for bounded flows have been successfully developed, e.g. Theofanous & Sullivan (1982) and Yuan & Michaelides (1992). Note that when $Re_b$ is large enough that $C_d$ and $C_v$ are approximately constant, $St_m$ is closely related to $\beta$ in that $\tau_b$ is proportional to $d_b/V_{term}$ and $\delta$ is proportional to $\Lambda$. It should be noted that $St_m$, $Fr_\delta$ and $\beta$ may only indicate different mechanism regimes, whereas the two quantities below may indicate the degree of $\delta$ modification.

The two recently developed momentum-based parameters for characterizing shear layer growth rates include: the drag loading ($D_L$) and the stability parameter ($A$). Drag loading is defined as the ratio of the dispersed phase drag on an eddy normalized by the Lagrangian change in momentum of the eddy due to its downstream motion (Davis 1993). The steady-state drag due to a single bubble is approximately $(\pi/6)\rho_f g d_b^3$, where $\rho_f$ is the density of the continuous fluid. The volume of liquid in a large eddy, assuming the eddy is cylindrical in shape and the void fraction is small, is $(\pi/4)\delta^2 w$, where $w$ is the width of the test section. The total number of bubbles per eddy, $N_b$, is then $3\epsilon\delta^2 w/(2d_b^3)$, where $\epsilon$ is the void fraction, from which we may determine the total bubble drag on the eddy. The Lagrangian change in momentum of an eddy (since it increases in size as it convects) can be expressed as

$$\frac{D(mV)}{dt} = \frac{\rho_f \pi w V_c^2 \delta^2}{2x}$$

where $x$ is the downstream distance from the virtual origin and $V_c$ is convective velocity of an eddy; thus drag loading can be expressed as $\epsilon g(x - x_o)/(2V_c^2)$, which is interestingly independent of bubble size.

The stability parameter, $A$, comes from non-dimensionalizing the interphase momentum transport term in the momentum equation for an incompressible inviscid mixing layer, assuming the dispersed phase is uniformly distributed and $\beta \ll 1$ (Yang *et al.* 1990). This study employed linear stability analysis to examine the amplitude of the most unstable wavelengths for a two-phase shear layer, and determined that increasing concentrations of the dispersed phase (increases in $A$) leads to increasing stabilization. While developed for particles, the equivalent expression for bubbles becomes $A = \epsilon g\delta/(V_c V_{rel})$. Note for Stokesian bubbles, $A$ becomes proportional to $\alpha C_v/\mathrm{St}$, which is related to the bubbly flow analogy of a parameter identified by Eaton (1994) for the uniformly dispersed interphase dissipation of the continuous phase turbulent energy. In addition, $D_L$ can be expressed as a function of $A$ and $V_{rel}/V_c$, where this velocity ratio was identified by Theofanous & Sullivan (1982) to predict turbulent energy modulation in pipe flow.

## 2. EQUIPMENT AND METHODOLOGY

The objective of the present investigation was to examine changes in the shear layer thickness when the bubble size becomes significant compared to the size of the surrounding fluid eddies. This experimental set-up provided time-averaged images of the shear layer with and without monodisperse bubbles, which were then studied quantitatively through digital image analysis. The test flowfield was a planar mixing layer with a uniform dilute bubble concentration across the high-speed side. A planar mixing layer was selected because its eddy structure is more coherent and accessible than other basic turbulent shear flows and has been widely documented as a single-phase flow. For the present test conditions, the Reynolds number based on shear layer thickness ranged from 10,000 to 70,000 indicating a fully developed turbulent shear layer (Koochesfahani *et al.* 1979). Test conditions were designed to straddle both the critical value of $\beta$ (0.07) suggested by Gore & Crowe (1989) as well a Stokes number of unity. These conditions included two nominal bubble diameters (2 and 4 mm), three convective velocities (0.3, 0.6 and 1.1 m/s), various streamwise positions ranging from 40 to 90 cm from the virtual origin, and void fractions up to 4%. For such conditions, the further complications associated with bubble–bubble interaction are expected to be small.

A Kemf & Remmers stainless steel closed return water tunnel was modified to generate a free shear layer with bubble injection on the high speed side. The test section has a cross sectional area of 25 × 25 cm and total length of 120 cm, where the tunnel was rotated 90° so that the buoyancy force would be in the streamwise direction. The flow was driven with a low turbulence in-line impeller 10 m upstream of the test section, capable of convective velocities of up to 2 m/s. A 9:1 contraction section just before the test section reduced test section turbulence levels (outside of the shear layer) to one percent or less (based on LDV measurements for the single-phase flow). The design of the splitter plate and pressure drop screens on the low-speed side (figure 1) was based on a similar configuration by Dimotakis & Brown (1976) and resulted in a velocity ratio of 0.24 ($V_2/V_1$).

The bubble injection system created an approximately uniform dispersion of air bubbles with void fractions of up to 4% within the shear layer. The bubbles were generated from a spanwise series of tubes protruding through the trailing edge of four streamwise NACA 0010 hydrofoils located upstream of the contraction, so as to not disturb the high speed flow. Tube IDs were 0.25 and 0.50 mm and the yielded bubble diameters were of approximately 2 and 4 mm, respectively. The bubble sizes were measured photographically, and it was found that 90% of the bubble diameters fell within ±0.5 and ±1.0 mm of these averages, respectively. The average void fraction in the shear layer at several streamwise locations was then determined based on photographic measurements of bubble density and calibrated volumetric flow meter readings, which yielded an uncertainty of ±10% or less. Note across the majority of the shear layer, bubble dispersion yielded void fraction uniformity to within ±10%, i.e. preferential bubble concentration was only weakly observed. In fact, bubble trajectories maintained roughly the same wobble

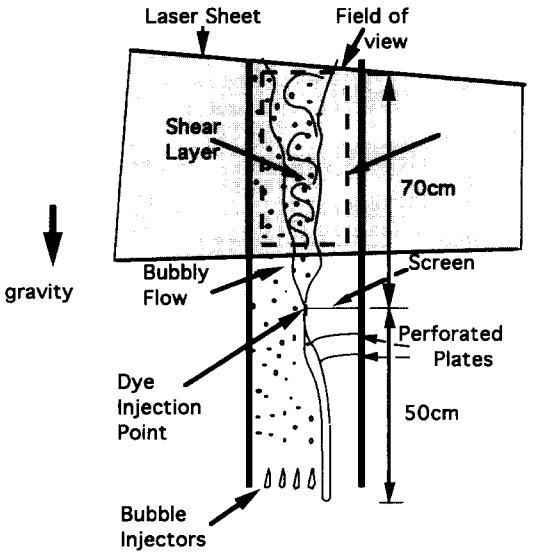


Figure 1. Splitter plate assembly, test section field of view, and LIF optical set up.

amplitude and frequency as their quiescent rising bubble counterparts, and "coring" (bubbles collecting along spanwise vortex cores) accounted for roughly 10% of the bubbles.

Laser induced fluorescence (LIF) is a non-intrusive flow visualization method which was utilized in this study to obtain both time-averaged shear layer thicknesses and temporally resolved videos of the shear layer dynamics. The flow was illuminated with an all-lines (blue/green) 5-W argon-ion laser sheet achieved by passing its beam through a cylindrical lens and a series of mirrors to illuminate the shear layer in the streamwise direction (figure 1). Disodium fluorescien dye was used as it is readily excited by such a laser and emits light at different wavelengths (yellow–orange). A dye injection port at the splitter tip yielded a marker for flow ingested into the shear layer by turbulent entrainment, thereby denoting the planar shear layer thickness.

Time averaged mixing layer images were then obtained by photographing through a standard argon-ion laser filter (to eliminate bubble or particle reflected light) with a 35 mm camera using a 2 s exposure time (consistent with a minimum of 10 $\tau_f$ for the present flow conditions). The filtered photographic images were then digitized and processed to yield transverse intensity profiles averaged over 1 cm streamwise intervals. The time-averaged shear layer thickness ($\delta$) was then defined as the distance between the two transverse points at which the intensity (referenced from the local minimum) was 30% of the maximum intensity values. Since this definition of $\delta$ was likely to be close to $\Lambda$ of the shear layer, we will redefine $\beta$ herein as $d_b/\delta$ for convenience. These $\delta$ values were then normalized by values from similarly processed images where no bubbles (NB) were injected into the flow, such that the net change in the shear layer thickness for each condition was simply taken to be $\delta/\delta_{NB}$. In addition to the time averaged visualization, time resolved video images were also obtained to observe the large scale structure modifications caused by the bubble addition. Further details of the facility and experimental techniques are given in Cebrzynski (1994).

## 3. RESULTS AND DISCUSSION

The single-phase cases yielded shear layer images which were consistent with planar images of scalar fields of other fully developed unforced free shear layers (e.g. Koochesfahani *et al.* 1979). Figure 2(a) and (b) shows typical 2s time-averaged images of the shear layer (used for obtaining widths) at an upstream without and with bubbles, respectively. Figure 2(c) and (d) shows typical instantaneous images of the shear layer (used for analyzing structures) at a downstream location without and with bubbles, respectively. Note, some bubbles are visible in figure 2(d), as the instantaneous images were not photographically filtered. In the figures, the flow is shown moving left to right with the high speed fluid above (although the actual flow is vertically upwards). In

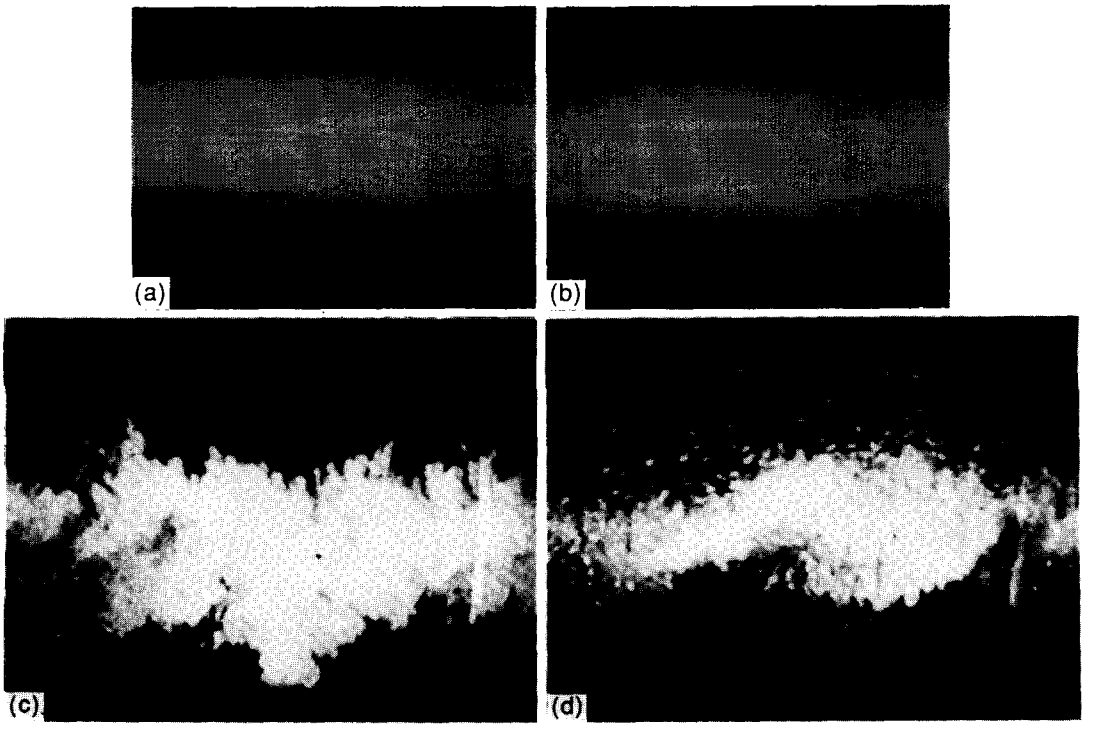


Figure 2. Planar images of the shear layer from video sequence for two sets of flow conditions: time-averaged images with a convection velocity of 53 cm/s with streamwise positions from 35 to 47 cm from splitter plate: (a) single-phase and (b) void fraction of 2.1% with 4 mm bubbles ($\delta/\delta_{NB}$ found to be 1.04); and instantaneous images with a convection velocity of 26 cm/s with streamwise positions from 60 to 71 cm from splitter plate; (c) single-phase and (d) void fraction of 3.4% with 2 mm bubbles ($\delta/\delta_{NB}$ found to be 0.77).

general, it was found that the influence of bubbles could lead to either an increase [figure 2(b)] or decrease [figure 2(d)] in the shear layer thickness. From the videos, it was noted that the thickness modification was correlated with changes in the shear layer coherency. Conditions which produced a decrease in thickness when bubbles were introduced ($\delta/\delta_{NB} < 1$) typically exhibited more coherent structures, often with clearly defined braids and eddies, e.g. figure 2(d). This was opposite of what was expected, i.e. it was initially thought that any improved coherency caused by the bubbles would increase the shear layer thickness as per excited single-phase results of Ho & Huang (1982). However, the increased coherency may indicate reduced three-dimensionality, which is consistent with a reduction in shear layer growth rates (Lowery 1986).

To determine the conditions which might affect the shear layer thickness modification, $\delta/\delta_{NB}$ was compared with the dimensionless parameters mentioned in the introduction. We will first examine the momentum based parameters which may indicate the degree of modification: $D_L$ and $A$. Increased drag loading displayed a significant tendency to decrease $\delta$ (figure 3), which is in qualitative agreement with Davis (1993) for particles in air. The idea is that greater "loads" on the mixing layer impede growth through damping the eddy dynamics and causing $\delta/\delta_{NB} < 1$. While there is significant scatter of the data about this trend, such variations are consistent with the significant uncertainties in measuring $\delta/\delta_{NB}$, i.e. $\pm 8\%$. However, the principle on which $D_L$ is based cannot account for the observed increases at low drag loadings. A possible mechanism for this increase will be discussed later with reference to the Stokes number. Also shown in figure 3 is a data point from Roig *et al.* (1993) for 2 mm bubbles with $V_1 = 52$ cm/s, $V_2 = 25$ cm/s, $x = 35$ cm, $\epsilon = 1.9\%$, $\delta$ NB $\sim 8.3$ cm and $\delta \sim 20.0$ cm. This data point is fundamentally different from the trend seen by the present data despite a similar upward flowing bubbly planar shear layer set-up. The reason for this difference is not clear, however it should be noted that their flow set-up yielded unusually high single-phase turbulence levels outside of the shear layer, i.e. 6–7% of $\Delta V$ vs 1% for the present flow. In addition, the present results are based on a passive scalar field as opposed to direct measurements of the velocity field.

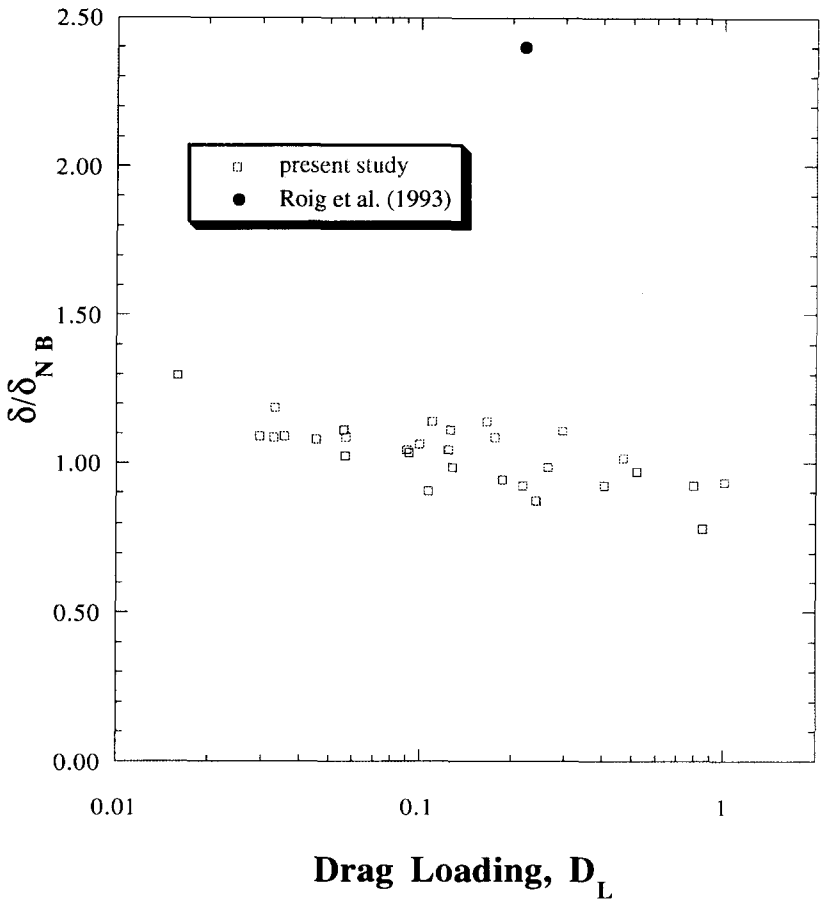


Figure 3. Drag loading vs non-dimensionalized shear layer thickness.

The thickness dependence on the stability parameter of Yang *et al.* (1990) also showed qualitative (weak) correlation of decreasing shear layer thickness with reduced amplification ratio (Cebrzynski & Loth 1995), based on the general expression given in the Introduction section and the values in table 1. The trend was consistent with that for the predicted ratio of the most amplified linear disturbance growth rates for two-phase as compared to single phase ($A = 0$), but the predicted growth rate ratios exhibited much stronger decreases, e.g. ratios were below 1/2 for most of the conditions given by the present study (which ranged from 0.01 to 0.2).

Next, we examine the influence of the dispersion length and time scales ($\beta$ and $St_m$), which may indicate mechanism regimes. The relationship between $\delta/\delta_{NB}$ and $\beta$ (which ranged from 0.03 to 0.14) indicates some support of a critical value of $\beta$ equal to 0.07, with 85% of the data falling within their prescribed regions and the other 15% never exceeding 10% above or below unity (as opposed to the maximum change of 35%). This trend is somewhat surprising since Gore & Crowe used local turbulent energies (which include PTM), whereas this study focused on overall turbulent entrainment, which is related to SITM. However, the overall correlation is not as strong as that given by $D_L$.

Stokes number dependence was examined in this study, even though it is primarily an indicator of bubble dispersion, because of the potential link between turbulence dispersion and turbulence modulation. The plot of $St_m$ versus $\delta/\delta_{NB}$ (figure 4) indicates a direct relationship between an increase in thickness and an increase in $St_m$. In fact, for $St_m \sim 1$, $\delta/\delta_{NB}$ is always greater than unity. Previous computational investigations, e.g. Ruetch & Meiburg (1993) have suggested that a St of roughly unity is an important transition for which bubble trajectories begin to display large deviations from streamlines. In addition, bubble wobble frequencies ($\sim 7$ Hz) were found to roughly correspond to $1/(2\tau_b)$. Therefore, since the Stokes number relates the timescale of the bubbles to the timescale of the continuous fluid large scale structures, the strong bubble wakes may

Table 1. Test conditions processed in this study

| $d_b$ (mm) | $u_1$ (cm/s) | $u_2$ (cm/s) | $x - x_o$ (cm) | $\epsilon$ | $\delta$ (cm) | $\delta_{NB}$ (cm) |
|---|---|---|---|---|---|---|
| 2.0 | 42 | 10.5 | 71 | 1.7 | 7.6 | 9.8 |
| 2.0 | 85 | 21.2 | 60.5 | 0.5 | 5.8 | 5.6 |
| 2.0 | 85 | 21.2 | 60.5 | 0.9 | 5.9 | 5.6 |
| 2.0 | 85 | 21.2 | 60.5 | 1.2 | 5.9 | 5.6 |
| 2.0 | 85 | 21.2 | 74 | 0.8 | 6.0 | 6.6 |
| 2.0 | 85 | 21.2 | 74 | 1.4 | 6.3 | 6.6 |
| 2.0 | 85 | 21.2 | 79 | 1.8 | 6.8 | 7.8 |
| 2.0 | 154 | 38.5 | 61 | 0.9 | 5.3 | 4.8 |
| 2.0 | 154 | 38.5 | 61 | 1.1 | 5.3 | 4.8 |
| 4.0 | 42 | 10.5 | 45.5 | 0.7 | 4.9 | 5.3 |
| 4.0 | 42 | 10.5 | 45.5 | 1.3 | 4.9 | 5.3 |
| 4.0 | 42 | 10.5 | 45.5 | 2.5 | 4.9 | 5.3 |
| 4.0 | 85 | 21.2 | 54 | 0.6 | 5.0 | 4.5 |
| 4.0 | 85 | 21.2 | 54 | 1.2 | 5.1 | 4.5 |
| 4.0 | 85 | 21.2 | 54 | 1.8 | 5.1 | 4.5 |
| 4.0 | 85 | 21.2 | 72 | 0.8 | 6.3 | 5.9 |
| 4.0 | 85 | 21.2 | 72 | 1.4 | 6.4 | 5.9 |
| 4.0 | 85 | 21.2 | 72 | 2.4 | 6.5 | 5.9 |
| 4.0 | 85 | 21.2 | 78 | 0.8 | 7.1 | 7.7 |
| 4.0 | 85 | 21.2 | 78 | 1.8 | 7.0 | 7.5 |
| 4.0 | 85 | 21.2 | 78 | 3.7 | 7.1 | 7.5 |
| 4.0 | 85 | 21.2 | 90 | 0.8 | 7.9 | 8.0 |
| 4.0 | 85 | 21.2 | 90 | 1.7 | 7.9 | 8.0 |
| 4.0 | 85 | 21.2 | 90 | 3.3 | 7.8 | 8.0 |
| 4.0 | 154 | 38.5 | 43 | 0.7 | 4.4 | 3.4 |
| 4.0 | 154 | 38.5 | 43 | 1.5 | 4.0 | 3.4 |
| 4.0 | 154 | 38.5 | 43 | 2.4 | 4.5 | 3.4 |
| 4.0 | 154 | 38.5 | 68 | 0.9 | 5.5 | 5.0 |
| 4.0 | 154 | 38.5 | 68 | 1.6 | 5.5 | 5.0 |
| 4.0 | 154 | 38.5 | 68 | 3.5 | 5.6 | 5.0 |
| 4.0 | 154 | 38.5 | 81.5 | 2.1 | 6.6 | 6.4 |
| 4.0 | 154 | 38.5 | 81.5 | 1.1 | 6.9 | 6.4 |

provide excitation of the shear layer ($\delta/\delta_{NB} > 1$) for $St_m$ of order unity as per Ho & Huang (1982). While temporal promotion of pairing and shear layer increases have been found for direct numerical simulations of shear flows with large bubbles of $St_m$ of order unity (Taeibi-Rahni *et al.* 1995), there is no direct experimental evidence to support this proposed mechanism. In fact, the lack of strong coherent structures associated with increase in shear layer thickness does not advance this conclusion.

A few other parameters including void fraction, eddy Froude number and shear layer Reynolds number were investigated to discern their possible correlation with changes in shear layer thickness (Cebrzynski & Loth 1995). Void fraction plotted versus $\delta/\delta_{NB}$ yielded a graph which appeared as a random scatter plot, which can be noted from table 1. Thus, void fraction only seems to have a role in characterizing other parameters, e.g. collecting test conditions and thickness ratios for void fractions of $1.6 \pm 0.2\%$ will consistently recover the previously noted trends for $D_L$, $A$, $\beta$, $St_m$. Examining the mixing layer Reynolds number influence on $\delta/\delta_{NB}$, also yielded no consistent trend. However, previous investigators, e.g. Serizawa *et al.* (1974), found modulation variations to be small with respect to $Re_\delta$ and therefore not likely to be noted given the uncertainty of the present data. The eddy Froude number (which ranged from 0.15 to 3.5) yielded a similar, but weaker, correlation as given by $St_m$, in that increases in $\delta/\delta_{NB}$ were associated with higher $Fr_\delta$. Finally, as stated earlier, the bubble distribution was approximately uniform for the streamwise variations of the test conditions, and eddy "coring" based on video images accounted for only for a small fraction of the bubbles, especially far downstream where the $Fr_\delta$ was small. This was consistent with results of Ruetch & Meiburg (1993) for bubble trajectories in a periodic Stuart vortex flow with similar $Fr_\delta$ and St, despite the complexity of the coherent structures in the present turbulent shear layer.

## 4. CONCLUSIONS

This study employed a closed-circuit vertical water tunnel modified to create a mixing layer with approximately uniform concentrations of ellipsoidal bubbles. Laser induced fluorescence and

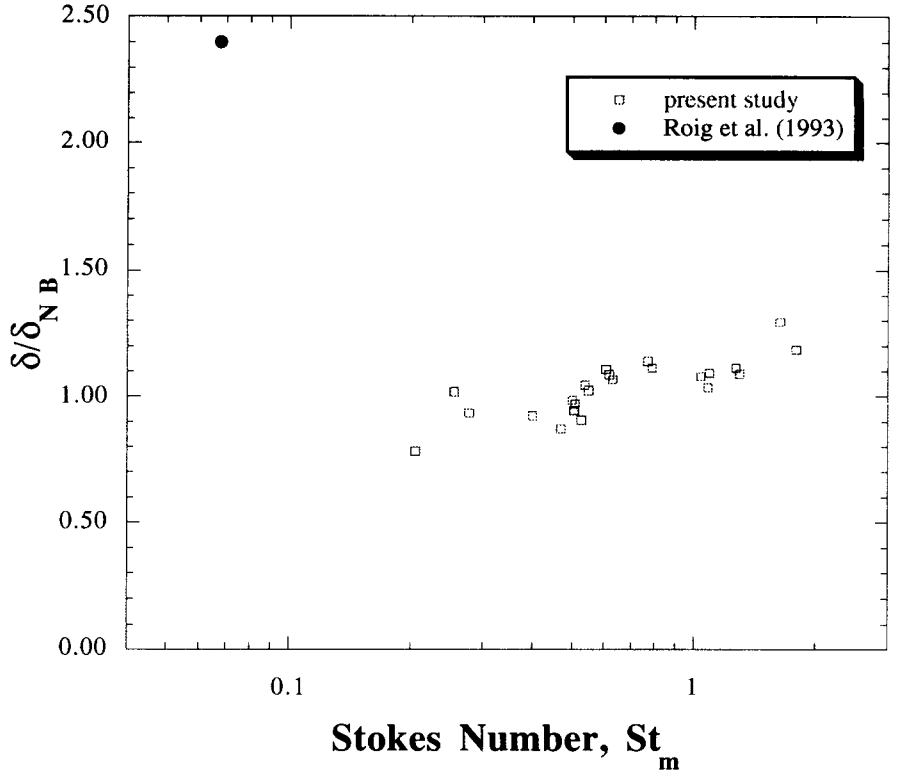


Figure 4. Modified Stokes number vs non-dimensionalized shear layer thickness.

digital image analysis was used to determine the shear layer thickness for both single-phase and bubbly flow conditions. In general, it was found that decreases in the passive scalar shear layer thickness were qualitatively associated with increased eddy and braid coherency and higher drag loadings, whereas increases in thickness were observed for Stokes numbers of order unity and supercritical dispersion length scale ratios, perhaps due to bubble wake excitation of the flow.

*Acknowledgements*—This research was funded by the Office of Naval Research under contract N00014-92-J-1157 with Dr Edwin Rood as technical monitor. The authors would also like to thank Franz Davis, whose research on digital analysis and multiphase mixing layers was modified for use in this study.

## REFERENCES

Cebrzynski, M. S. 1994 Turbulence modulation of a bubbly free shear layer. M.Sc. thesis, University of Illinois at Champaign Urbana, Urbana, IL.

Cebrzynski, M. S. & Loth, E. 1995 Changes in the thickness of a free shear layer due to large bubbles. *Proceedings of the International Symposium on Gas–Liquid Two-phase Flows.*

Davis, F. D. 1993 Visualization of turbulence modulation with large particles. M.Sc. thesis, The University of Illinois at Champaign Urbana, Urbana, IL.

Dimotakis, P. E. & Brown, G. L. 1976 The mixing layer at high reynolds number: large-structure dynamics and entrainment. *J. Fluid Mech.* **78,** 535–560.

Dimotakis, P. E. 1991 Turbulent free shear layer mixing and combustion. *Prog. Astronautics Aeronautics* **137,** 265–340.

Eaton, J. K. 1994 Experiments and simulations on turbulence modification by dispersed particles. *Appl. Mech. Rev.* **46,** S44–49.

Gore, R. A. & Crowe, C. T. 1989 Effect of particle size on modulating turbulence intensity. *Int. J. Multiphase Flow* **15,** 279–285.

Hestroni, G. 1993 The effect of particles on the turbulence in a boundary layer. In *Particulate Two-Phase Flow* (Edited by Roco, M. C.), pp. 244–264. Butterworth–Heinemann, Boston, MA.

Ho, C-M. & Huang, L-S. 1982 Subharmonics and vortex merging in mixing layers. *J. Fluid Mech.* **119,** 443–473.

Jiang, B., Varty, R. L. & Sigurdson, L. W. 1993 The acceleration of a single bubble rising from a nozzle in water. *Fluid Engng Div. ASME* **165,** 161–169.

Koochesfahani, M. M., Catherasoo, C. J., Dimotakis, P. E., Gharib, M. & Lang, D. B. 1979 Two-point LDV measurements in a plane mixing layer. *AIAA J.* **17,** 1347–1351.

Lopez de Bertodano, M., Lahey Jr, R. T. & Jones, O. C. 1994 Development of a $k$–$\epsilon$ model for bubbly two-phase flow. *Trans. ASME* **116,** 128–134.

Lowery, P. 1986 Numerical simulation of a spatially-developing, forced, plane mixing layer. Ph.D. thesis, Department of Mechanical Engineering, Stanford University, Stanford, CA.

Roig, V., Suzanne, C. & Masbernat, L. 1993 Measurements in a two-phase mixing layer. *Proceedings of Experimental Heat, Fluid Mechanics, and Thermodynamics* (Edited by Kelleher, M. D. *et al.*), pp. 1342–1348. Elsevier, Amsterdam.

Ruetch, G. R. & Meiburg, E. 1993 On the motion of small spherical bubbles in two-dimensional vortical flows. *Phys. Fluids* **5,** 2326–2341.

Serizawa, A., Kataoka, I. & Michiyoshi, I. Turbulence structure of air–water bubbly flow—II. Local properties. *Int. J. Multiphase Flow* **2,** 235–246.

Stewart, C. W. & Crowe, C. T. 1993 Bubble dispersion in free shear layers. *Int. J. Multiphase Flow* **19,** 501–507.

Taebi-Rahni, M., Loth, E. & Tryggvason, G. 1995 Flow modulation of a planar free shear layer with large bubbles-direct numerical simulations. *Int. J. Multiphase Flow*. In press.

Theofanous, T. G. & Sullivan, J. 1982 Turbulence in two-phase dispersed flows. *J. Fluid Mech.* **116,** 343–362.

Tio, K.-K., Liñán, A., Lasheras, J. C. & Gañán-Calvo, A. M. 1993 The dynamics of bubbles in periodic vortex flows. *Appl. Scient. Res.* **51,** 285–290.

Yang, Y., Chung, J. N., Troutt, T. R. & Crowe, C. T. 1990 The influence of particles on the spatial stability of two-phase mixing layers. *Phys. Fluids A* **2,** 1839–1845.

Yuan, Z. & Michaelides, E. E. 1992 Turbulence modulation in particulate flows—a theoretical approach. *Int. J. Multiphase Flow* **18,** 779–785.